

Stability Certification Standards for DC Microgrid Networks with Arbitrary Load Configurations

Samuel Chevalier, *Student Member, IEEE*, Kathleen Cavanagh, *Student Member, IEEE*, Konstantin Turitsyn, *Member, IEEE*, Luca Daniel, *Member, IEEE* and Petr Vorobev, *Member, IEEE*,

Abstract—DC microgrids are prone to small-signal instabilities due to the presence of tightly regulated loads. This paper develops a decentralized stability certificate which is capable of certifying the small-signal stability of an islanded DC network containing such loads. Utilizing a novel homotopy approach, the proposed standards ensure that no system eigenmodes are able to cross into the unstable right half plane for a continuous range of controller gain levels. The resulting “standards” can be applied to variety of grid components which meet the specified, but non-unique, criteria. These standards thus take a step towards offering *plug-and-play* operability of DC microgrids. The proposed theorems are explicitly illustrated and numerically validated on a test-case example of a DC microgrid network containing controlled buck converter loads.

Index Terms—Constant power load, microgrids, parameterization, small-signal stability, stability criteria.

I. INTRODUCTION

RECENT advances in power electronics technologies and the general trend towards renewable energy sources have lead to increased interest in DC grids [1], [2]. Small-scale DC microgrids have been in use for several decades already, mainly as autonomous electric systems on board of vehicles [3]. As such, the configuration of these microgrids was fixed and well planned for the exact operating conditions which were known in advance. On the other hand, DC microgrids with an “open” structure, capable of being expanded and reconfigured while remaining stable for a broad range of loading conditions, have mostly been out of the scope of academic research. In part, this is justified by the fact that, currently, the majority of microgrids are using an AC interface for power distribution, even if all the sources and loads are naturally DC. However, fully DC microgrids can become an economically feasible solution for supplying power in remote communities.

Unlike in AC grids where a substantial part of the load is of the electro-mechanical type, loads in DC grids are mostly represented by power electronics converters with tight controls to achieve flat voltage at their outputs [4]. This leads to a constant power load (CPL) behavior on the input within the control loop bandwidth, which is regarded to be one of the main sources of instabilities in DC grids. The origin of the instability is often related to the, so-called, negative incremental resistance introduced by CPL; a number of methods for stability assessment are based on such representation. Recent reviews [5], [6] present a comprehensive classification of the existing stability criteria and stabilization methods for DC grids.

Recently, the problem of stability assessment for CPL-based microgrids has attracted substantial attention from the

controls community [7]–[11]. In our previous works on the subject [12]–[14], we have demonstrated that the problem of linear and transient stability of DC microgrids with CPL can be addressed using Brayton-Moser mixed potential approach [15], [16]. However, stability conditions derived under the conservative CPL modeling assumption may lead to excessive constraints on network configuration and installed equipment, and they neglect the complex dynamical behaviour of the controllers which regulate these loads. In reality, regulated power converters act similar to CPL only within their control loop bandwidth [17]. Accordingly, methods which explicitly account for the finite bandwidth of load controllers can potentially provide less restrictive stability conditions. However, dealing with load models that are more complex than a simple CPL requires development of rather specific techniques.

Traditionally, the power electronics community has relied on a number of different impedance based stability conditions. Most of them consider the minor loop gain, which is the ratio of the source output impedance to the load input impedance. The celebrated Middlebrook criterion [18], originally proposed for input filter design, is based on a small-gain condition for minor loop gain, demanding its absolute value to be less than unity for all frequencies. While a rather conservative method, it only requires knowledge of the absolute values of impedances over the whole frequency range. A less conservative Gain-Margin Phase-Margin criterion [19] allows the Nyquist plot of the minor loop gain to leave the unit circle provided there is a sufficient phase margin. Another method - the opposing argument criterion - is based on conditions imposed on the real part of the minor loop gain [20]. The main advantage of this method is that it can be applied to multi-load systems, since the contributions from each individual load can now be simply added together. Finally, the least conservative methods are based on the so-called energy source consortium analysis (ESCA) [21] and the similar root exponential stability criterion (RESC) [22]. Both offer the smallest forbidden region for the minor loop gain of all the existing methods.

Most of the described stability assessment methods are primarily concerned with single-source single-load systems and a possible destabilizing interaction between the impedances of corresponding components. Under certain conditions, it could be possible to generalize some of these methods by attributing network components to either loads or sources and changing the corresponding effective impedance. In all the cases, the explicit knowledge of both the models of all the system components and the network configuration are required to perform the stability assessment. However, in the

case of the aforementioned “open structure” DC grids, not all of the parameters can be exactly known. Moreover, running a separate stability test upon every grid reconfiguration can be practically infeasible. Thus, there is the need for stability assessment methods that can be realized under limited knowledge about the system parameters and/or configuration. In the present manuscript, we have made a step towards offering a “plug-and-play” approach for DC grids, where certain general criteria can be issued for both loads and network elements that can guarantee stable operation of the full system under arbitrary grid configurations. To achieve this end, we develop a specialized procedure that allows for the overall system stability assessment to be reduced to a separate consideration for individual load and line impedances, thus resulting in completely decentralized stability criteria.

The main contributions of the manuscript are as follows:

- 1) We propose a novel homotopic parameterization of closed loop load controller gains that can track the regions where small-signal stability is lost.
- 2) Based on the above parametrization, we develop a fully decentralized stability criteria which can be applied to DC grids with different components (i.e. sources, lines, and loads) and can certify stability for an arbitrary network configuration of these components.
- 3) We prove that any component which satisfies this criteria can be safely added to a network without a system eigenmode crossing into the unstable right half plane, thus allowing for “plug-and-play” operability of DC microgrids.

II. TECHNICAL BACKGROUND

In this section, the small-signal model of a constant power DC load is recalled. Next, a small-signal DC microgrid network model is stated, and the problem of certifying the network’s stability is outlined.

A. Constant Power DC Load Model

DC-DC power electronic converters are designed with a control system which properly mitigates input voltage variations in order to provide a fairly constant load voltage. A common way to represent a lossless converter is using a single-pole, double-throw (SPDT) switch with a duty cycle D . Due to the switch, which operates with a frequency on the order of tens of kilohertz, the inductor current and capacitor voltage vary throughout a given cycle with small amplitude around their average values even in steady state. Therefore, to properly account for the low frequency variations, the so-called small-ripple approximation is used, where the system is averaged over a given period and switching variations are neglected.

While there are several common types of converters, we will focus on the buck converter due to its prevalence. The buck converter, consisting of an inductance L , capacitance C and constant resistance load R , has a step-down conversion ratio D . Since averaging is done over many switching periods, an ideal DC transformer, rather than a switch, is used in the small-signal model. Further buck converter details are provided in [4]. To maintain constant voltage at its output, a converter

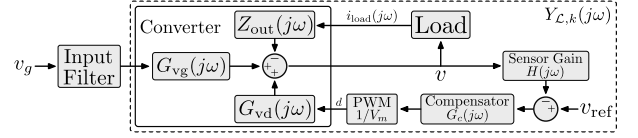


Fig. 1: Definition of Small-Signal Load Model

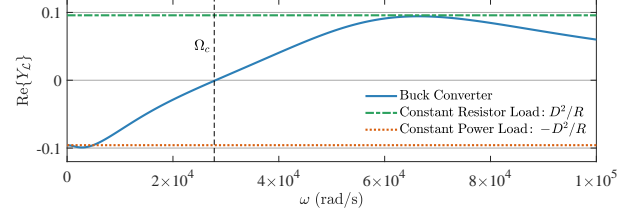


Fig. 2: Shown are the real parts of the input admittance for a buck converter (blue), constant resistance load (green), and constant power load (orange).

relies on feedback to modify the duty cycle following any variations in the input voltage. In this work, we consider a buck converter interfaced with a constant resistance on its output and a control loop to stabilize the output voltage. In this way, it is seen from the network as a constant power load in steady state. This model is defined in Fig. 1. To characterize the small-signal behavior of the buck converter, we first examine the transfer function from the control input (duty cycle variation) $d(s)$ to the output voltage $v(s)$ [4]:

$$G_{vd}(s) = \frac{v(s)}{d(s)} = G_{d0} \frac{\omega_0^2}{s^2 + 2\zeta\omega_0 s + \omega_0^2} \quad (1)$$

with $G_{d0} = V/D$, $\omega_0 = 1/\sqrt{LC}$ and $\zeta = \sqrt{L/C}/(2R)$. In the presence of voltage control, the loop gain of the system is defined as $T = G_{vd}(s)H(s)G_c(s)/V_m$, where H is the sensor gain, $G_c(s)$ is the compensator transfer function and V_m is the voltage of the pulse width modulation. The compensator is modeled as a simple lead-lag controller of the form

$$G_c(s) = G_{c\infty} \frac{(1 + \frac{\omega_L}{s})(1 + \frac{s}{\omega_z})}{(1 + \frac{s}{\omega_p})} \quad (2)$$

The input admittance transfer function $Y_{L,k}(s)$ can be written

$$Y_{L,k}(s) = \frac{i(s)}{v_g(s)} = \frac{1}{Z_N(s)} \frac{T(s)}{1+T(s)} + \frac{1}{Z_D(s)} \frac{1}{1+T(s)}, \quad (3)$$

where, for a buck converter,

- $Z_N = \frac{-R}{D^2}$ is the converter impedance when the load voltage perturbations $v(s)$ are eliminated (i.e. $d(s)$ is infinitely fast and the load acts like constant power), and
- $Z_D = \frac{R}{D^2} \frac{1+sL/R+s^2LC}{1+sRC}$ is the converter impedance in the absence of control input $d(s)$ (i.e. the load acts like constant impedance).

In steady state, $Z_D = -Z_N$. This is shown quite clearly by the green and orange traces in Fig 2, where above Ω_c , $\text{Re}\{Y_L(\omega)\} > 0$, and the load behaves more like a passive impedance. In practice, converters are also equipped with an input filter to reject the high-frequency current components from converter switching actions. Improper input filter design can bring instability to an otherwise stable converter.

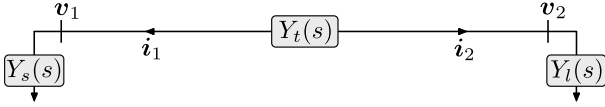


Fig. 3: Simple 2 bus DC microgrid network. The source, load, and line dynamics are represented by $Y_s(s)$, $Y_l(s)$, and $Y_t(s)$, respectively.

B. Network Modeling for Small-Signal Stability Analysis

To study the small-signal stability of the full DC microgrid, we leverage a network whose connected graph $G(\mathcal{V}, \mathcal{E})$ has edge set \mathcal{E} with cardinality $|\mathcal{E}| = m$, vertex set \mathcal{V} with cardinality $|\mathcal{V}| = n$, and signed nodal incidence matrix $E \in \mathbb{R}^{m \times n}$. This network has a set of operating equilibrium voltages $\mathbf{V}_0 \in \mathbb{R}^n$ and nodal current injections $\mathbf{I}_0 \in \mathbb{R}^n$. The vectors of voltage and current perturbations are written as $\mathbf{v}(t) = \mathbf{V}(t) - \mathbf{V}_0$ and $\mathbf{i}(t) = \mathbf{I}(t) - \mathbf{I}_0$, respectively. Finally, the Laplace domain representations of these signal vectors are written as $\mathbf{v}(s) = \mathcal{L}\{\mathbf{v}(t)\}$ and $\mathbf{i}(s) = \mathcal{L}\{\mathbf{i}(t)\}$.

Next, we define the frequency dependant nodal admittance matrix according to the general rule

$$\mathbf{i}(s) = \mathbf{Y}(s)\mathbf{v}(s). \quad (4)$$

Matrix $\mathbf{Y}(s)$ includes contributions from the network matrix $\mathbf{Y}_N(s)$ and the diagonal shunt¹ matrix \mathbf{Y}_S . Written explicitly,

$$\mathbf{Y}(s) = \sum_{\{i,j\} \in \mathcal{E}} \mathbf{Y}_N^{(i,j)}(s) + \sum_{i \in \mathcal{V}} \mathbf{Y}_S^{(i)}(s), \quad (5)$$

where $\mathbf{Y}_N^{(i,j)}$ is the matrix associated with the network connection between buses i and j , and $\mathbf{Y}_S^{(i)}$ is the matrix associated with shunt elements at bus i . For example, the simple network illustrated in Fig. 3 can be decomposed and written as

$$\mathbf{Y} = \mathbf{Y}_N^{(1,2)} + \mathbf{Y}_S^{(1)} + \mathbf{Y}_S^{(2)} \quad (6a)$$

$$= \begin{bmatrix} Y_t & -Y_t \\ -Y_t & Y_t \end{bmatrix} + \begin{bmatrix} Y_s & 0 \\ 0 & 0 \end{bmatrix} + \begin{bmatrix} 0 & 0 \\ 0 & Y_l \end{bmatrix}. \quad (6b)$$

If $\mathbf{Y}_L(s)$ is the diagonal matrix of line admittances, then (5) can also be conventionally expressed via $\mathbf{Y}(s) = E^T \mathbf{Y}_L(s) E + \mathbf{Y}_S(s)$. In the absence of external perturbations,

$$\mathbf{0} = \mathbf{Y}(s)\mathbf{v}(s) \quad (7)$$

will always be satisfied, since the network obeys Kirchhoff's laws. In general, (7) may only be satisfied by nontrivial solutions of $\mathbf{v}(s)$ when $s = s_0$ is chosen such that $\mathbf{Y}(s_0)$ is a singular matrix.

Definition 1. $\mathbf{v}e^{s_0 t}$, $\mathbf{v} \neq \mathbf{0}$, is an *eigenmode* of $\mathbf{Y}(s)$ if

$$\mathbf{0} = \mathbf{Y}(s_0)\mathbf{v}e^{s_0 t}. \quad (8)$$

In the following, both s_0 and $\mathbf{v}e^{s_0 t}$ will be referred to as the same eigenmode. As a necessary consequence of (8), $\det[\mathbf{Y}(s_0)] = 0$ if s_0 is an eigenmode. We now collect all values of s_0 which satisfy Definition 1 and place them in the vector \mathbf{s}_0 . The small-signal stability of system (4) can be gauged by computing the real parts of \mathbf{s}_0 .

¹Shunt elements are any elements which tie the network to ground, and they can include loads, sources, and network elements.

Lemma 1. *System (7) is stable if*

$$\text{R}\{s_0\} < 0, \forall s_0 \in \mathbf{s}_0. \quad (9)$$

The proof of Lemma 1 is located in Appendix A, along with the proofs of all remaining Lemmas and Theorems.

III. DECENTRALIZED STABILITY CERTIFICATES

In this section, the proposed small-signal network model is “parameterized” by scaling its closed loop controller gains. Leveraging this parameterization, a decentralized stability certificate is derived. This certificate is then updated to accommodate networks where negative admittances are present at zero frequency. Finally, a simple, tractable example is given in order to illustrate the mechanics behind the proposed methods.

A. Centralized Stability Assessment via Parameterization

We choose to “parameterize” our network model with a homotopic scalar gain value $\alpha \in [0, 1]$, where $\alpha = 1$ corresponds to a nominal (or desired) system configuration. Next, we appropriately multiply α by all closed loop controller gains in the network which influence stability. For example, if the open loop admittance of a dynamical load is given by $h(s)$, and proportional feedback control is added, its closed loop admittance may be computed as

$$Y(s) = \frac{h(s)}{1 + K \cdot h(s)}. \quad (10)$$

When this closed loop admittance is parameterized, the transfer function may be written as

$$Y(s, \alpha) = \frac{h(s)}{1 + (\alpha \cdot K) \cdot h(s)}. \quad (11)$$

Clearly, when $\alpha = 0$, the closed feedback loop is broken. The primary feature of this parameterization scheme is that for $\alpha = 0$, the system is “definitely” stable, i.e. all of its eigenmodes are in the LHP. This claim can be certified by considering that, when $\alpha = 0$, all relevant controller gains (voltage regulation, power sharing, etc.) in the network are set to 0. When this occurs, all of the closed loop feedback mechanisms in the network are effectively broken. The system will thus be operating in a definitely stable, open loop configuration. When α is scaled up to 1, then all of the controller gains have also been scaled up to their nominal values. As will be clarified, the scaling of α from 0 to 1 can be thought of as a homotopy procedure, since it represents a smoothly varying parameterization of the system eigenmodes.

Using this parameterization scheme, matrix $\mathbf{Y}(s, \alpha)$ represents the previously derived small-signal network model which has been parameterized with α . The general strategy for proving the stability of the system $\mathbf{Y}(s, \alpha)$ is based on the well-known “zero exclusion principle” and is closely related to the μ -analysis, as is shown in the following stability lemma.

Lemma 2. *Assuming $\mathbf{Y}(s, \alpha)$ is stable for $\alpha = 0$, then $\mathbf{Y}(s, \alpha)$ is also stable for $\alpha = 1$ if the determinant satisfies*

$$\det[\mathbf{Y}(s = j\omega, \alpha)] \neq 0, \forall \omega \geq 0, \forall \alpha \in [0, 1]. \quad (12)$$

To generalize this lemma, we introduce the rotational function

$$\mathcal{D}(\omega, \alpha) = e^{j\phi(\omega, \alpha)} \quad (13)$$

whose magnitude is unity and whose phase function $\phi(\omega, \alpha)$ depends on both frequency and the parameterization value α .

Remark 1. *The results of lemma 2 remain valid if $\mathbf{Y}(s, \alpha)$ is multiplied by any nonzero function. Thus, we can write the generalization of condition (12) as*

$$\det[\mathcal{D}(\omega, \alpha)\mathbf{Y}(s = j\omega, \alpha)] \neq 0, \quad \forall \omega \geq 0, \quad \forall \alpha \in [0, 1]. \quad (14)$$

While (14) can guarantee the stability of the system $\mathbf{Y}(s, \alpha)$, it is centralized in nature, i.e., there is no way to relate the determinants of the subsystems with the determinant of the full system. Rather than require a nonzero determinant, a more restrictive condition is to require the positive definiteness of the matrix over the same range. While conservative, positive definiteness has a very useful additive property, i.e., if the matrices in a set are all positive definite, then so is their sum.

Lemma 3. *Assume network $\mathbf{Y} \equiv \mathbf{Y}(s, \alpha)$ is stable for $\alpha = 0$. Set $s = j\omega$. If there exists $\mathcal{D} \equiv e^{j\phi(\omega, \alpha)}$ for which*

$$\mathcal{D}\mathbf{Y} + (\mathcal{D}\mathbf{Y})^\dagger \succ 0, \quad \forall \omega \geq 0, \quad \forall \alpha \in [0, 1], \quad (15)$$

then $\mathbf{Y}(s, \alpha)$ is stable for all gain values up to $\alpha = 1$.

B. Decentralized Stability Rules

As written, (15) is still a fully centralized stability certificate, because \mathbf{Y} is the full system matrix. The certificate can be converted to a decentralized stability certificate, though, by writing \mathbf{Y} as a summation of its network and shunt components, as in (5). To simplify notation, we introduce set $\mathcal{C} = \mathcal{E} \cup \mathcal{V}$; it is defined to be the set of indices associated with all dynamical elements in the network. Furthermore, $Y_k \equiv Y_k(s, \alpha)$, $k \in \mathcal{C}$ refers to the k^{th} complex scalar transfer function element in the system (line, load, or source).

Theorem 1. *Assume network $\mathbf{Y} \equiv \mathbf{Y}(s, \alpha)$ of (7) is stable for $\alpha = 0$. Set $s = j\omega$. If there exists $\mathcal{D} \equiv e^{j\phi(\omega, \alpha)}$ for which*

$$\text{Re}\{\mathcal{D}Y_k\} > 0, \quad \forall k \in \mathcal{C}, \quad \forall \omega \geq 0, \quad \forall \alpha \in [0, 1], \quad (16)$$

then $\mathbf{Y}(s, \alpha)$ is stable for all gain values up to $\alpha = 1$.

As a helpful simplification, we may use polar coordinates to write $\theta_k \equiv \angle Y_k(\omega, \alpha)$ and $|Y_k| \equiv |Y_k(\omega, \alpha)|$. Thus, the positivity condition in (16) can be stated as

$$0 < \mathcal{D}Y_k + (\mathcal{D}Y_k)^\dagger \quad (17a)$$

$$= 2|Y_k| \text{Re}\{e^{j(\phi(\omega, \alpha) + \theta_k)}\}. \quad (17b)$$

Using (17), we have the following corollary.

Corollary 1. *If there exists $\phi \equiv \phi(\omega, \alpha)$ for which*

$$-\frac{\pi}{2} < \phi + \theta_k < \frac{\pi}{2}, \quad \forall k \in \mathcal{C}, \quad \forall \omega \geq 0, \quad \forall \alpha \in [0, 1], \quad (18)$$

and $\mathbf{Y}(s, \alpha = 0)$ is stable, then $\mathbf{Y}(s, \alpha = 1)$ is also stable.

C. The Problem of Negative Admittance at Zero Frequency

Assuming the network model is constructed using physical laws and physically realizable controllers, the admittance matrix $\mathbf{Y}(s = j0, \alpha)$ will be a purely real matrix. Therefore, the angle θ_k associated with all elements in this matrix will have an angle of either $\theta_k = 0^\circ$ or $\theta_k = 180^\circ$. If any shunt element, such as a constant power load, has $\theta_k = 180^\circ$ at $s = j0$, then condition (18) cannot be satisfied at this frequency, since any network line will necessarily have $\theta_k = 0^\circ$. Mathematically, this limiting case of $s = j0$ cannot be ignored, since a negative real eigenmode (i.e. system pole) may potentially travel on the real axis and cross the imaginary axis at $s = j0$. Therefore, network singularity at zero frequency must be considered.

Definition 2. *System $\mathbf{Y}(s, \alpha)$ is said to be zero-frequency stable if $\det[\mathbf{Y}(s = j0, \alpha)] \neq 0, \forall \alpha \in [0, 1]$. That is, no real eigenmode crosses into the RHP as α is scaled from 0 to 1.*

We note, however, that $\det[\mathbf{Y}(s = j0, \alpha)] = 0$ will occur at the point of maximum network loadability. Therefore, if this determinant is close to 0, then the system is operating on the tip of the so-called ‘‘nose curve’’. Practical systems are engineered to operate far from this nose curve. We therefore offer the following assumption, which entirely precludes the possibility of a system encountering zero-frequency instability.

Assumption 1. *System (7) is assumed to operate far from the steady state nose curve and is therefore zero-frequency stable.*

With the addition of Assumption 1, we update Corollary 1.

Corollary 2. *If there exists $\phi \equiv \phi(\omega, \alpha)$ for which*

$$-\frac{\pi}{2} < \phi + \theta_k < \frac{\pi}{2}, \quad \forall k \in \mathcal{C}, \quad \forall \omega > 0, \quad \forall \alpha \in [0, 1], \quad (19)$$

and Assumption 1 holds, and $\mathbf{Y}(s, \alpha = 0)$ is stable, then $\mathbf{Y}(s, \alpha)$ is also stable $\forall \alpha \in [0, 1]$.

Per (19), the phase condition must be satisfied for all positive ω , rather than all non-negative ω , as in (18).

D. Numerical Example

As an illustrative example, we consider the network in Fig. 3. We define the open-loop load dynamics via

$$h(s) = \frac{1}{s^2 + 2\zeta\omega_n s + \omega_n^2}. \quad (20)$$

A PI controller is then added in a negative feedback loop to yield the resulting admittance function

$$Y_l(s) = \frac{h(s)}{K(1 + \frac{1}{s\tau_i})h(s) + 1}. \quad (21)$$

The source is considered to be an ideal voltage source² connected through a short line. Thus, the admittances associated with the source and the network line are respectively given by

$$Y_s(s) = \frac{1/R_s}{1 + s\tau}, \quad Y_t(s) = \frac{1/R_l}{1 + s\tau}, \quad (22)$$

²Ideal voltage sources act as direct paths to ground in an admittance model.

where, for simplicity, the time constant τ is assumed equal in both admittances. We consider the stability of this system in two ways: first, using the non-conservative centralized approach of Lemma 2, and second, using the decentralized approach proposed by Corollary 2.

1) *Centralized Stability Approach:* In the centralized approach of Lemma 2, we may leverage the full, centralized network model. Rather than scaling α , we directly scale gain value K to determine its maximal tolerable value. The determinant of system admittance matrix (6) is

$$\det[\mathbf{Y}] = (Y_s + Y_t)(Y_l + Y_t) - Y_t^2. \quad (23)$$

Satisfying $(Y_s + Y_t)(Y_l + Y_t) - Y_t^2 = 0$ simplifies to

$$s^3 + (\tau R + 2\zeta\omega_n)s^2 + (\omega_n^2 + K + R)s + K/\tau_i = 0, \quad (24)$$

where $R \equiv R_s + R_l$. By Routh-Hurwitz, an eigenmode will become unstable when $K > \tau_i(\tau R + 2\zeta\omega_n)(\omega_n^2 + K + R)$. This simplifies to

$$K > \frac{\tau_i(\tau R + 2\zeta\omega_n)(\omega_n^2 + R)}{1 - \tau_i(\tau R + 2\zeta\omega_n)} \equiv \hat{K} \quad (25)$$

assuming $1 > \tau_i(\tau R + 2\zeta\omega_n)$. When (25) is satisfied as an equality, the complex roots of (24) are

$$s = 0 \pm j\sqrt{(\omega_n^2 + R)/(R\tau\tau_i + 2\tau_i\zeta\omega_n - 1)} \equiv j\hat{\omega}. \quad (26)$$

Since $\det[\mathbf{Y}(s = j\hat{\omega})] = 0$ for $K = \hat{K}$, this is the gain value for which stability is lost, and $\hat{\omega}$ is the frequency of the system mode that becomes unstable. When applying the numerical values $\omega_n = 2\pi$, $\zeta = 0.1$, $\tau = 0.1$, and $\tau_i = 0.25$, we find $\hat{K} = 20.77$ is the maximum tolerable gain value.

2) *Decentralized Stability Approach:* In the decentralized approach, we consider positive definiteness of the network elements independently via condition (19). To apply this corollary, we parameterize the load by setting $K \rightarrow \alpha \cdot \hat{K}$, so that for $\alpha = 1$, the system will definitely become marginally stable. Next, we independently define the phase functions $\theta_t(\omega, \alpha)$ and $\theta_l(\omega, \alpha)$ associated with parameterized admittance functions $Y_t(\omega, \alpha)^3$ and $Y_l(\omega, \alpha)$:

$$\theta_t(\omega, \alpha) = \tan^{-1}(-\omega\tau) \quad (27)$$

$$\theta_l(\omega, \alpha) = \tan^{-1}\left(\frac{\alpha \cdot \hat{K}/\tau_i - 2\zeta\omega_n\omega^2}{\omega(\omega_n^2 + \alpha \cdot \hat{K}) - \omega^3}\right). \quad (28)$$

Next, we plug these phase functions into inequality (18). We then plot the range of values which the unknown function $\phi(\omega, \alpha)$ can permissibly take, for each element, as *continuous* functions of frequency and as *discrete* functions of α . The results are shown in Fig. 4. In panel (f), it can clearly be seen that the inequality “breaks” at $\omega \approx 7.59$. This corresponds to $\alpha = 0.871$ with a corresponding maximum controller gain of $K \approx 18.1$. When the sectors lose continuous overlap, the inequality is necessarily violated, and stability of the interconnection can no longer be guaranteed (even though the system damping ratio is still 0.8%). While $K \approx 18.1$ is 12.9% conservative, this gain value guarantees stability not only for

³Since they have identical time constants, the line and the source phase functions are identical. Thus, only one of them is defined.

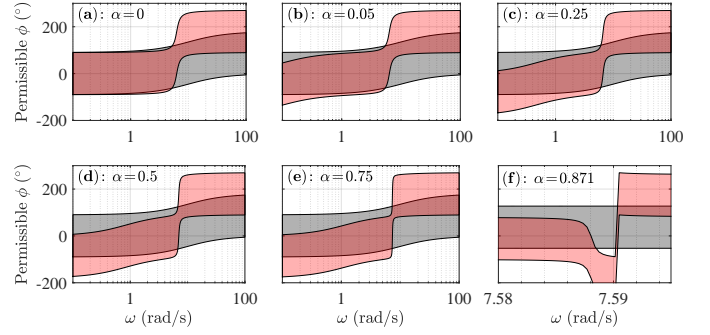


Fig. 4: The shaded regions are the values that function $\phi(\omega, \alpha)$ can take, according to inequality (19), for a continuum of frequency and controller gain values. The grey sector corresponds to the line phase function (27), while the red sector corresponds to the load phase function (28). Loss of overlap between these shaded regions indicates the non-existence of function $\phi(\omega, \alpha)$.

the circuit in Fig. 3, but also for an arbitrary interconnection of an arbitrary number of components in that circuit (assuming the system is still zero-frequency stable). Thus, it provides a generalized stability guarantee, rather than just a specific one.

IV. NUMERICAL TEST RESULTS

In this section, we consider a microgrid system consisting of three primary components: stiff battery-based voltage sources, RL lines, and constant resistance loads connected to buck converters. In the first subsection, we initialize the 8-bus microgrid system of Fig. 5. Next, we appropriately parameterize the buck converters. Finally, we analyze the small-signal stability of the network under two different controller configurations.

A. System Initialization

We first consider the equilibrium point of the network, since this operating point will influence the input voltage V for the loads. The specific details of network initialization are found in Appendix B. To introduce variety into the network, the line lengths are chosen from a normal distribution with a small standard deviation: $l_{ij} = 1 + \mathcal{N}(0, 0.1^2)$. Solving (40) using the parameter values provided in Table I, we get a solution with non-source nodal voltages ranging from 28.8V to 29.3V.

B. Buck Converter Parameterization

In the microgrid system of Fig. 5, the loads are modeled as constant resistance and are interfaced with the network through buck converters. The nominal converter and controller parameters have been drawn from [4] and are defined in Table I. The buck converter’s transfer function, with the additional grounded filter capacitor from Fig. 1, can be parameterized by scaling the compensator gain $G_{c\infty}$ from (2). Thus,

$$G_c(s, \alpha) \equiv \alpha \cdot G_c(s) \quad (29)$$

and the full transfer function can be written as

$$Y_{\mathcal{L}_c}(s, \alpha) \triangleq \frac{V_m D^2}{V_m + G_c(s, \alpha) G_{vd}(s) H} \left(\frac{1 + sRC}{R + sL + s^2RLC} - G_c(s, \alpha) \frac{G_{vd}(s) H}{RV_m} \right) + C_{fs}, \quad (30)$$

	Parameter	Description	Value
Converter	V	Input Voltage	28 ~ 30 V
	R	Load Resistance	3 Ω
	C	Capacitance	500 μF
	L	Inductance	50 μH
	D	Duty Cycle	0.536
Controller	$G_{c\infty}$	Midband Gain	3.7
	w_L	Lead Zero	$2\pi \cdot 500$ Hz
	w_z	Trailing Zero	$2\pi \cdot 1700$ Hz
	w_p	Pole	$2\pi \cdot 14.5$ kHz
	H	Sensor Gain	1/3
	V_m	Voltage of PWM	4
Network	C_f	Filter Capacitor	500 μF
	l_{ij}	Line Length	1.0 km
	r	Line Resistance	0.2 Ω/km
	τ	Line Time Constant	1 ms
	V_s	Source Voltage	30 V

TABLE I: Converter, Controller, and Network Parameters

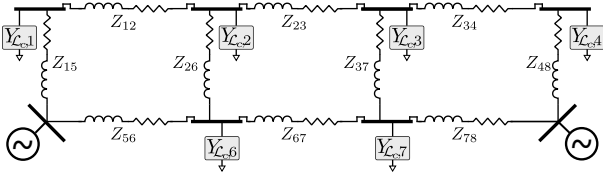


Fig. 5: Meshed 8-bus microgrid with two stiff voltage sources and six loads.

where C_f represents the parallel filter capacitor. At non-zero frequencies, when $\alpha \rightarrow 0$, (30) relaxes to

$$Y_{\mathcal{L},c}(s, \alpha \rightarrow 0) = D^2 \left(\frac{1 + sRC}{R + sL + s^2RLC} \right) + C_f s, \quad (31)$$

which is effectively a passive RLC transfer function. Thus, the associated parameterized system will be *definitely stable* when $\alpha = 0$. When $s \rightarrow j\omega$, the admittance relaxes to

$$Y_{\mathcal{L},c}(s \rightarrow j\omega, \alpha) = -D^2/R, \quad (32)$$

as would be expected from a constant power load. Since the zero frequency response of the load is negative, the conditions from Corollary 2 must be satisfied in order to certify the stability of the network in Fig. 5. In this system, the generators are assumed to be stiff, battery-based voltage sources. Accordingly, their only dynamics are captured by the interconnecting line. The phase response of the RL lines (including the source lines) is given according to

$$\theta_Z(\omega, \alpha) = \tan^{-1}(-\tau\omega), \quad (33)$$

where $\tau = L/R$. The phase response of (30) is analytically cumbersome, but it can be numerically computed as

$$\theta_{\mathcal{L}}(\omega, \alpha) = \tan^{-1} \left(\frac{\text{Im} \{Y_{\mathcal{L}}(s = j\omega, \alpha)\}}{\text{Re} \{Y_{\mathcal{L}}(s = j\omega, \alpha)\}} \right). \quad (34)$$

C. Testing Network Stability

We now gauge the stability of the network under two buck converter controller configurations: a lead-lag filter, as in (3), and a common PI filter. In both cases, stability assessments are performed using an exact, centralized approach (i.e. root locus), and via the decentralized approach of Corollary 2.

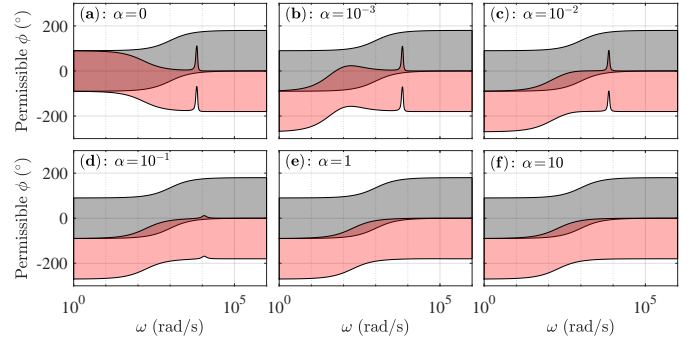


Fig. 6: Plotted are the values that $\phi(\omega, \alpha)$ can take, according to (19), for a continuum of frequency and gain values. The grey sector corresponds to the line phase function (33), while the red sector corresponds to the load phase function (34), where $G_c(s)$ is a lead-lag controller.

1) *Lead-Lag Controller*: In this example, $G_c(s)$ is the lead-lag controller specified in (3). According to [4], the stability of (3) is primarily controlled by the roots of $1 + T(s)$. With the parameters from Table I, the lead-lag filter gives the bode plot of $1 + T(s)$ a phase margin of $\phi_m = 45.6^\circ$ and a gain margin of $g_m = \infty$. Using this controller, we first apply the decentralized approach of Corollary 2 by analyzing the phase functions (33) and (34). These results are shown in Fig. 6, where the phase functions are plotted from $\alpha = 0$ up to $\alpha = 10$ (i.e. scaling the gain $G_{c\infty}$ to 10 times its nominal value). As can be seen, there exists continuous overlap between the sectors; this is true for all loads in the system (results not shown), despite the small differences in equilibrium input voltages for the loads. Since the network is “definitely stable” for $\alpha = 0$, Corollary 2 is satisfied, and the system is *guaranteed stable under arbitrary interconnection*, assuming input voltages remain sufficiently close to those tested (i.e. within a few volts).

Next, we confirm these results using Lemma 1 and testing the system eigenmodes on a root locus plot as α is scaled. To do so, we build the parameterized system admittance matrix $\mathbf{Y}(s, \alpha) \in \mathbb{C}^{8 \times 8}$ and construct the N^{th} order polynomial $\det[\mathbf{Y}(s, \alpha)] = 0$, where $N = 40$. Finally, we employ the MATLAB root solver `roots()` to build the complex vector

$$\mathbf{s}(\alpha) = \{s \mid \det[\mathbf{Y}(s, \alpha)] = 0\}. \quad (35)$$

As shown in Fig. 7, no eigenmodes cross into the RHP for any value of $\alpha \leq 10$. Therefore, the conclusion of Corollary 2 is correct: the network is stable for any gain value $G_{c\infty}$, even up to 10 times its nominal value. Of course, we have confirmed the prediction only for a single network configuration, but the results should generalize to an arbitrary network configuration. To further confirm this result, we set $\alpha = 10$ and applied a 0.5 Volt step increase to the voltage source set point at bus 5. The resulting stable dynamic responses are shown in Fig. 8.

2) *PI Controller*: In this test, we used a PI controller:

$$G_c(s) = G_i \left(1 + \frac{\omega_i}{s} \right). \quad (36)$$

Setting $\omega_i = 2\pi 500$ and $G_i = 0.015$, the phase and gain margins of $1 + T(s)$ were driven to $\phi_m = 93.6^\circ$ and $g_m = 12.3$ dB. The resulting phase function analysis results are shown in Fig. 9, where the phase functions are plotted from $\alpha = 0$ up to $\alpha = 7$ (i.e. scaling the gain $G_{c\infty}$ to 7 times its nominal

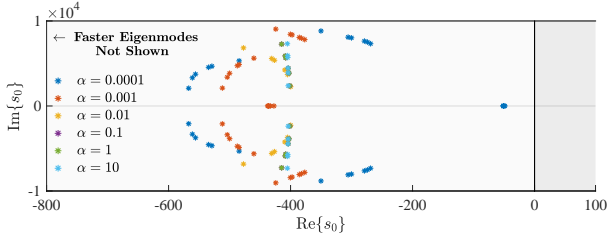


Fig. 7: Eigenmode locus of the Fig. 5 microgrid via (35). All buck converters are outfitted with lead-lag controllers. Stability is never lost for $\alpha \leq 10$.

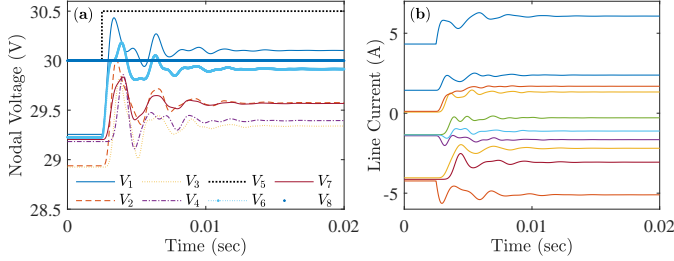


Fig. 8: Shown are the nodal voltage (panel (a)) and line current (panel (b)) dynamic responses for a 0.5V step change in supply voltage at source bus 5. Despite the large controller gain values associated with $\alpha = 10$, system settling time is on the order of 10ms.

value). As can be seen, there is a break in continuous overlap between the sectors at $\alpha = 3.8$, corresponding to a **maximum allowable controller gain** of $3.8 \times 0.015 = 0.057$. The root locus plot is shown in Fig. 10. The network is clearly still stable for $\alpha = 3.8$, but becomes marginally stable for $\alpha = 4.5$. Stability is clearly lost for larger value of α , as shown by the eigenmodes of $\alpha = 7$, for example. Therefore, Corollary 2 is conservative by a margin of $100 \times (1 - 3.8/4.7) \approx 20\%$ for this particular network configuration. In this context, the results of Fig. 9 can be interpreted alternatively: there exists some network configuration for which $\alpha = 3.8$ is the maximum allowable gain factor.

V. PRACTICAL APPLICATIONS TO THE DESIGN AND OPERATION OF DC MICROGRIDS

Although mathematical in nature, the results of Corollary 2 can lead to a plethora of (i) practical design guidelines for engineers and (ii) useful operational tools for non-expert microgrid users. Both are briefly considered.

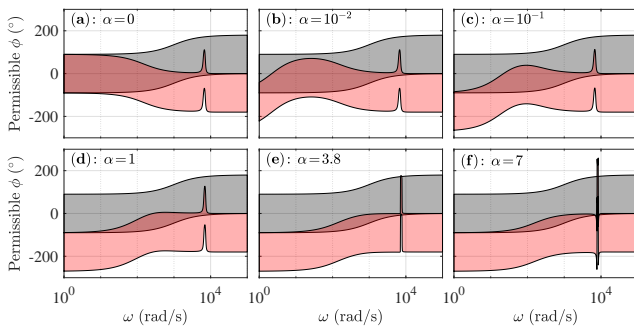


Fig. 9: Plotted are the values that $\phi(\omega, \alpha)$ can take, according to (19), for a continuum of frequency and gain values. The grey sector corresponds to the line phase function (33), while the red sector corresponds to the load phase function (34), where $G_c(s)$ is a PI controller.

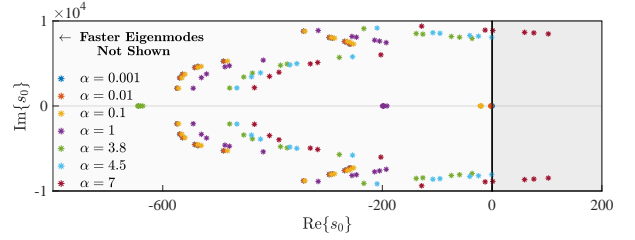


Fig. 10: Eigenmode locus of the Fig. 5 microgrid via (35). All buck converters are outfitted with PI controllers. System stability is lost when $\alpha > 4.5$.

1) *Microgrid Design Tools*: If an engineering team desires plug and play operability of a microgrid, they can follow the steps of Algorithm 1. This procedure can have three outcomes: it will either (i) confirm the plug-and-play operability of all desired elements, (ii) determine the maximum value of α for which the system can operate, or (iii) identify the components which must be removed in order for the system to operate at $\alpha = 1$ (i.e. nominal controller values).

Since the amount of overlap between phase curves implicitly parameterizes a stability margin, this procedure can also directly inform design constraints. For example, Fig. 6 was used to guarantee plug-and-play stability for constant power loads connected to RL lines. These results only hold, though, for the tested parameter values. If, for example, the time constant associated with the lines increased from $\tau = 1$ ms to $\tau = 7$ ms, all of the gray curves would shift backwards in frequency and overlap would be lost. Accordingly, an example of a practical design constraint follows:

- For plug-and-play operability to be achieved in a network with buck converter loads, lines must be chosen such that their electromagnetic time constants satisfy $\tau < 7$ ms.

Algorithm 1 Microgrid Design Procedure

Require: Candidate components Σ_i and potential input voltages V_j

- 1: **for** each microgrid component Σ_i **do**
- 2: **for** each potential input voltage V_j **do**
- 3: **for** a sufficient number of $\alpha \in [0, 1]$ values **do**
- 4: Parameterize closed loop gains of Σ_i with α
- 5: Compute **or** measure Σ_i 's phase response $\theta_i(\alpha, V_j, \omega)$
- 6: **end do**
- 7: **end do**
- 8: **end do**
- 9: **end do**
- 10: **end do**
- 11: **end do**
- 12: **end do**

11: **either** terminate at this α **or** remove non-overlapping item

12: **return** Maximum α and non-rejected Σ_i, V_j pairs

2) *Microgrid Operational Tools*: We consider a situation in which a variety of common microgrid components are collectively analyzed by Algorithm 1. Immediate analysis could be performed by design engineers or researchers, while future analysis could be performed directly by manufacturers. Any particular combination of microgrid elements which satisfy the criteria of Algorithm 1 can then be aggregated to form a particular "class". For user simplicity, each class can be associated with a color (i.e. "red class", "blue class", etc.). Of

course, any particular microgrid element can simultaneously belong to multiple classes, but mixing elements of certain classes could lead to instability. Depending on the needs of a microgrid, the designers could pre-determine the classes of elements which can be plug-and-play added to the microgrid without compromising the stability of the network. Users of the microgrid, then, would only need to check if a load, for example, satisfies the class designation of the microgrid. If it does, it can be safely added (i.e. plugged in) to any arbitrary location in the network without compromising stability.

VI. CONCLUSION

In this paper we have developed a fully decentralized small-signal stability criteria for DC networks that can allow for plug-and-play operability. We have demonstrated that placing certain constraints on the DC loads' controller gains and/or network elements can guarantee stable operation under their arbitrary interconnection. We believe that these results will have practical impact, such as by fostering the development of the ready-to-use standards for DC loads and/or sources, that can be directly used by industry.

APPENDIX A

Proof of Lemma 1. In the absence of external perturbations, the solution to (7) will be a scaled sum of its eigenmodes. The decay rate of each eigenmode is given by $\text{Re}\{s_0\}$. If (9) holds, then the solution will decay exponentially fast. \square

Proof of Lemma 2. For $\alpha = 0$, the real part of all eigenmodes will lie in the LHP. For the system to go unstable, an eigenmode must cross the imaginary axis. At the point of crossing, $\exists \alpha, \omega \ni \det[\mathbf{Y}(s = j\omega, \alpha)] = 0$, since one of the eigenmodes will necessarily have $\text{Re}\{s_0\} = 0$. If this does not occur, the system remains stable. \square

Proof of Lemma 3. Assume matrix \mathbf{Y} becomes singular for some allowed values of ω, α . Then $D\mathbf{Y}$ will also be singular, meaning $D\mathbf{Y} + (D\mathbf{Y})^\dagger$ cannot be positive definite. If (15) is satisfied, \mathbf{Y} cannot become singular, and Lemma 2 holds. \square

Proof of Theorem 1. Using (5), we break system $D\mathbf{Y}$ into

$$D\mathbf{Y} = \underbrace{\sum_{i,j \in \mathcal{E}} D\mathbf{Y}_N^{(i,j)}}_A + \underbrace{\sum_{i \in \mathcal{V}} D\mathbf{Y}_S^{(i)}}_B. \quad (37)$$

Assume (16) holds true. By construction, matrix $A_H = A + A^\dagger$ necessarily has a single $\lambda = 0$ eigenvalue, and all others are positive. The eigenvector associated with this zero eigenvalue is equal to $\mathbf{e} = [1, 1, \dots, 1]^\top$. Matrix $B_H = B + B^\dagger$ is also a PSD matrix, but it is additionally diagonal, so $\mathbf{e}^\dagger B_H \mathbf{e} > 0$. Thus, (16) implies positive definiteness of $D\mathbf{Y} + (D\mathbf{Y})^\dagger$, which further implies the stability of $\mathbf{Y}(s, \alpha)$ up to $\alpha = 1$. \square

APPENDIX B

To initialize the network in Fig. 5, we assume steady state ($\omega = 0$) operation. We then order the network such that buses 1 through n_s are source buses while buses $n_s + 1$ through n are load buses. We define Y_l as the diagonal matrix of line admittances, where each diagonal element is $1/r_{ij}$, and we define Y_s as the diagonal matrix of shunt (i.e. load) admittances, where each diagonal element is D^2/R (i.e. the negative of incremental resistance (32)). We further define

$$Y_b = E^\top Y_l E + Y_s \quad (38)$$

as the nodal admittance matrix. Next, we define \mathbf{V}_s as the vector of *known* source voltages, \mathbf{V}_l as the vector of *unknown* load voltages,

and \mathbf{I}_s as the vector of *unknown* current injections at the sources. Partitioning (38), we therefore have

$$\begin{bmatrix} Y_{b1} & Y_{b2} \\ Y_{b3} & Y_{b4} \end{bmatrix} \begin{bmatrix} \mathbf{V}_s \\ \mathbf{V}_l \end{bmatrix} = \begin{bmatrix} \mathbf{I}_s \\ \mathbf{0} \end{bmatrix}. \quad (39)$$

By re-arranging the bottom set of equations from (39), the unknown steady state voltages may be computed as

$$\mathbf{V}_l = -Y_{b4}^{-1} Y_{b3} \mathbf{V}_s. \quad (40)$$

REFERENCES

- [1] E. Planas, J. Andreu, J. I. Gárate, I. M. de Alegría, and E. Ibarra, "Ac and dc technology in microgrids: A review," *Renewable and Sustainable Energy Reviews*, vol. 43, pp. 726–749, 2015.
- [2] J. J. Justo, F. Mwasilu, J. Lee, and J.-W. Jung, "Ac-microgrids versus dc-microgrids with distributed energy resources: A review," *Renewable and Sustainable Energy Reviews*, vol. 24, pp. 387–405, 2013.
- [3] A. Emadi, M. Ehsani, and J. M. Miller, *Vehicular electric power systems: land, sea, air, and space vehicles*. CRC press, 2003.
- [4] R. W. Erickson and D. Maksimovic, *Fundamentals of power electronics*. Springer Science & Business Media, 2007.
- [5] S. Singh, A. R. Gautam, and D. Fulwani, "Constant power loads and their effects in dc distributed power systems: A review," *Renewable and Sustainable Energy Reviews*, vol. 72, pp. 407–421, 2017.
- [6] A. Riccobono and E. Santi, "Comprehensive review of stability criteria for dc distribution systems," in *Energy Conversion Congress and Exposition (ECCE), 2012 IEEE*, pp. 3917–3925, IEEE, 2012.
- [7] S. Sanchez, R. Ortega, G. Bergna, M. Molinas, and R. Grino, "Conditions for existence of equilibrium points of systems with constant power loads," in *2013 IEEE 52nd Annual Conference on Decision and Control (CDC)*, pp. 3641–3646, IEEE, 2013.
- [8] J. W. Simpson-Porco, F. Dörfler, and F. Bullo, "On Resistive Networks of Constant-Power Devices," *IEEE Transactions on Circuits and Systems II: Express Briefs*, vol. 62, no. 8, pp. 811–815, 2015.
- [9] J. Zhao and F. Dörfler, "Distributed control and optimization in DC microgrids," *Automatica*, vol. 61, pp. 18–26, Nov. 2015.
- [10] N. Barabanov, R. Ortega, R. Grino, and B. Polyak, "On Existence and Stability of Equilibria of Linear Time-Invariant Systems With Constant Power Loads," *IEEE Transactions on Circuits and Systems I: Regular Papers*, vol. 63, no. 1, pp. 114–121, 2016.
- [11] C. De Persis, E. R. Weitenberg, and F. Dörfler, "A power consensus algorithm for dc microgrids," *Automatica*, vol. 89, pp. 364–375, 2018.
- [12] J. A. Belk, W. Inam, D. J. Perreault, and K. Turitsyn, "Stability and control of ad hoc dc microgrids," in *Decision and Control (CDC), 2016 IEEE 55th Conference on*, pp. 3271–3278, IEEE, 2016.
- [13] W. Inam, J. A. Belk, K. Turitsyn, and D. J. Perreault, "Stability, control, and power flow in ad hoc dc microgrids," in *Control and Modeling for Power Electronics (COMPEL), 2016 IEEE 17th Workshop on*, pp. 1–8, IEEE, 2016.
- [14] K. Cavanagh, J. A. Belk, and K. Turitsyn, "Transient Stability Guarantees for Ad Hoc DC Microgrids," *IEEE Control Systems Letters*, vol. 2, no. 1, pp. 139–144, 2018.
- [15] R. Brayton and J. Moser, "Some Results on the Stability of Nonlinear Networks Containing Negative Resistances," *IEEE Transactions on Circuit Theory*, vol. 11, no. 1, pp. 165–167, 1964.
- [16] D. Jeltsema and J. Scherpen, "Multidomain modeling of nonlinear networks and systems," *IEEE Control Systems Magazine*, vol. 29, no. 4, pp. 28–59, 2009.
- [17] A. M. Rahimi and A. Emadi, "An analytical investigation of dc/dc power electronic converters with constant power loads in vehicular power systems," *IEEE Transactions on vehicular technology*, vol. 58, no. 6, pp. 2689–2702, 2009.
- [18] R. Middlebrook, "Input filter considerations in design and application of switching regulators," *IEEE IAS Annual Meeting*, 1976.
- [19] C. M. Wildrick, F. C. Lee, B. H. Cho, and B. Choi, "A method of defining the load impedance specification for a stable distributed power system," *IEEE Transactions on power Electronics*, vol. 10, no. 3, pp. 280–285, 1995.
- [20] X. Feng, J. Liu, and F. C. Lee, "Impedance specifications for stable dc distributed power systems," *IEEE Transactions on Power Electronics*, vol. 17, no. 2, pp. 157–162, 2002.
- [21] S. D. Sudhoff, S. F. Glover, P. T. Lamm, D. H. Schmucker, and D. Delisle, "Admittance space stability analysis of power electronic systems," *IEEE Transactions on Aerospace and Electronic Systems*, vol. 36, no. 3, pp. 965–973, 2000.
- [22] S. D. Sudhoff and J. M. Crider, "Advancements in generalized impedance based stability analysis of dc power electronics based distribution systems," in *Electric Ship Technologies Symposium (ESTS), 2011 IEEE*, pp. 207–212, IEEE, 2011.